Published in final edited form as:
Macromolecules. 2010 November 9; 43(21): 9094–9099. doi:10.1021/ma101434a.

Yielding Behavior in Injectable Hydrogels from Telechelic Proteins

Bradley D. Olsen, **Julia A. Kornfield***, and **David A. Tirrell***
California Institute of Technology Division of Chemistry and Chemical Engineering, Pasadena, CA 91125

Abstract

Injectable hydrogels show substantial promise for use in minimally invasive tissue engineering and drug delivery procedures.[1,2] A new injectable hydrogel material, developed from recombinant telechelic proteins expressed in *E. coli*, demonstrates shear thinning by three orders of magnitude at large strains. Large amplitude oscillatory shear illustrates that shear thinning is due to yielding within the bulk of the gel, and the rheological response and flow profiles are consistent with a shear-banding mechanism for yielding. The sharp yielding transition and large magnitude of the apparent shear thinning allow gels to be injected through narrow gauge needles with only gentle hand pressure. After injection the gels reset to full elastic strength in seconds due to rapid reformation of the physical network junctions, allowing self-supporting structures to be formed. The shear thinning and recovery behavior is largely independent of the midblock length, enabling genetic engineering to be used to control the equilibrium modulus of the gel without loss of the characteristic yielding behavior. The shear-banding mechanism localizes deformation during flow into narrow regions of the gels, allowing more than 95% of seeded cells to survive the injection process.

Introduction

Hydrogels are widely used in tissue engineering because of the similarity between their properties and those of native tissue.[3] Injectable hydrogels offer added advantages, in that they can be used in minimally invasive surgical procedures.[1, 2] In addition to meeting traditional tissue engineering design criteria (including tunable gel modulus and biological functionality[3–5]), injectable gels must flow under modest pressure and set rapidly at the target site. A variety of injectable materials have been developed either by chemically crosslinking the gel after injection[6–8] or by engineering the gel to undergo a temperature,[9–11] pH,[12] or ion-sensitive[2] transition between the sol and gel states. Alternatively, a few injectable materials based on shear-thinning hydrogels have been reported,[12–19] where a drop in the modulus of the gel at high shear rates allows it to flow during injection. Recovery of the elastic modulus after shear is potentially more rapid than chemical crosslinking or physically responsive gelation, providing for more uniform cell distributions in the injected gel[15] and greater control over placement of the material.[12] In addition, shear thinning materials can be engineered to form stable gel phases across wide ranges of temperatures and solution conditions, allowing environmentally stable formulations to be prepared long before use.

Although the biological properties and linear mechanics of tissue engineering hydrogels have been extensively investigated, the nonlinear rheology that leads to shear thinning and

*To whom correspondence should be addressed: tirrell@caltech.edu (DAT) or jak@cheme.caltech.edu (JAK).

injectability is less well understood. Dissociation of the physically associating groups under shear is clearly implicated in shear thinning behavior;[12–16] however, the flow profiles and mechanisms of thinning are often unknown. In particular, it has been extensively demonstrated for a wide variety of entangled systems, in particular polymer melts and wormlike micellar solutions, that inhomogeneous flow profiles may occur due to instabilities in the stress-strain curve.[20–25] These instabilities are manifest as shear bands, areas of high deformation rate where the entanglements are preferentially disrupted, that accommodate the majority of the strain applied to the system.

Tirrell and coworkers reported a system of biofunctional physical hydrogels designed from telechelic proteins[26] in which coiled-coil endblocks are joined by a flexible polyanionic linker (Figure 1), and the coiled-coil motif has been exploited in both telechelic[27–30] and graft polymers[31–33] to produce a wide variety of protein hydrogels. Protein engineering allows control of the coiled-coil association multiplicity in the network junctions, and changes in the coiled-coil sequence[29,30] and midblock molecular weight[28,34] can be used to vary the modulus of the hydrogel through changes in the relative fractions of looped and bridged chains in the gel. Functional sequences such as the RGD cell binding domain can be incorporated into the midblock through genetic engineering without affecting the physical properties of the materials.[35] Gel structures based on similar design paradigms have been reported for block copolypeptides,[36] elastin-mimetic triblock copolymers,[37–39] and telechelic proteins that use collagen-like blocks to form associating helical domains.[40,41]

Here we evaluate a model system of telechelic protein hydrogels as injectable materials, demonstrating striking shear-thinning behavior and nearly instantaneous recovery of full elastic strength after cessation of shear. The observed flow behavior is explained in terms of the formation of shear bands in the gel at high stress. Yielding of the gel promotes rapid recovery of the elastic modulus and allows encapsulated cells to survive injection by distributing strain inhomogeneously in the flowing material.

Experimental Methods

For expression of the proteins $PC_{10}P$ and $PC_{30}P$, the corresponding genes were incorporated into plasmids and transformed into *E. coli* strain SG13009 containing the pREP4 plasmid. The encoding $PC_{10}P$ (with an N-terminal 6×His tag) had already been prepared in the pQE-9 expression vector (Qiagen) by Shen et al.[30] (plasmid pQE9- $PC_{10}P$). The plasmid encoding $PC_{30}P$ was prepared by first digesting pQE9-C_{10} from Shen et al.[30] with *Spe*I and *Nhe*I to isolate the ~300 bp sequence encoding a C_{10} unit, then digesting pQE9-$PC_{10}P$ with *Spe*I and ligating the C_{10} sequence into it. The digestion and ligation procedure was repeated a second time to form pQE9-$PC_{30}P$. Expression was performed in TB media and cultures were seeded at a 1:100 dilution with a saturated starter culture. Cells were grown at 37 °C until OD_{600} reached 0.9–1.0, and then induced with 1.0 mM isopropyl β-D-1-thiogalactopyranoside (IPTG). Protein expression proceeded for five hours, after which the cells were harvested and lysed in 8 M urea. Cells were frozen at −80 °C, thawed, and sonicated. Cell lysates were clarified by centrifugation, and the proteins of interest were isolated using Ni-NTA affinity chromatography. Yields of $PC_{10}P$ and $PC_{30}P$ were approximately 130 mg/L culture, and purity was confirmed by denatured state polyacrylamide gel electrophoresis (SDS-PAGE) and matrix-assisted laser desorption ionization mass spectrometry (MALDI-MS). Protein sequences and gels are included in the supplemental information.

Gel samples were prepared by mixing lyophilized protein with 100 mM phosphate buffer with the pH adjusted to 7.6 for a total gel concentration of 7% w/v. Samples were held at 4 °C until the protein was fully hydrated, generally 2 to 4 hours, then heated above the sol-gel transition by immersion in a boiling water bath for 60 seconds. The gels were allowed to

reassociate under quiescent conditions at room temperature to erase any thermal and flow history. Rheological measurements were performed on a TA Instruments ARES-RFS strain controlled rheometer with a 25 mm diameter cone and plate geometry. The outer edge of the sample was coated in oil in order to slow evaporation; the linear rheological properties of the materials were found to be stable for more than 48 hours in this configuration. Linear rheological data were acquired at 10% strain amplitude (dynamic modulus, $G^*(\omega)$), and nonlinear rheological data were acquired using a fixed frequency (1 rad/s) that is in the elastic plateau region of $G^*(\omega)$. Time-dependent healing after cessation of large amplitude oscillatory shear (LAOS) was probed using 0.1% strain amplitude at 1 rad/s frequency.

Flow visualization experiments were performed on $PC_{10}P$ hydrogels using green fluorescent polystyrene microspheres (10 μm diameter) as tracer particles at 0.1 vol. %. The gel was loaded into a syringe and injected through a plastic capillary tube with 0.79 mm inner diameter using a syringe pump to control the nominal flow rate of the gel. Images were acquired on a Zeiss 510 inverted laser scanning confocal microscope according to the method of Fraser and coworkers.[42] Line scans perpendicular to the flow direction were acquired in a plane through the center of the capillary at 1.93 ms/line for 2000 scans in order to produce images of the flow.

CHO K1 cells were grown to ~80% confluence on tissue culture polystyrene in cell growth media. Cell passages 16–20 were used for experiments. Cells were trypsinized, pelleted, and resuspended in fresh media. The cell suspension was then added to lyophilized $PC_{30}P$ protein to make a total concentration of 7% w/v protein and gently stirred with the pipette tip. The mixture was placed on ice for two hours to allow hydration, at which time a nearly homogeneous and transparent gel had formed. The gel was loaded into a 1 mL syringe and injected through a 22 gauge needle onto a cover slip. The gel was placed on ice for 15 minutes, at which point it was covered completely in cell growth media containing 2 μM calcein and 4 μM ethidium D (EthD) from the Invitrogen live/dead assay kit. The cells were held for 45 minutes before imaging on a Zeiss 510 inverted laser scanning confocal microscope. The green channel was excited at 488 nm and the red channel was excited at 532 nm. DIC images were taken using 532 nm illumination.

Results and Discussion

The telechelic protein sequences PC_xP are constructed from two helical endblocks (denoted P) linked by x-repeats of the nonapeptide sequence (C): $PC_{10}P$ (20.5 kg/mol) has 10 nonapeptide repeats, while $PC_{30}P$ (36.6 kg/mol) has 30 nonapeptide repeats. The coiled-coil P domains associate into pentameric bundles due to a combination of hydrophobic and ionic interactions, forming physical crosslinks in the gels (Figure 1). Complete sequences of $PC_{10}P$ and $PC_{30}P$ are given in the Supporting Information.

While the linear rheology of the telechelic protein hydrogels is typical for physically gelling materials, the nonlinear rheology reveals strong shear-thinning behavior (Figure 2). In the linear regime, both $PC_{10}P$ (Figure 2a) and $PC_{30}P$ (Figure 2b) hydrogels exhibit plateaus in the elastic modulus, G', for frequencies above 0.1 rad/s. At fixed mass concentration, the magnitude of the plateau modulus decreases with increasing length of the protein midblock from $PC_{10}P$ to $PC_{30}P$—in contrast to the behavior observed earlier for tetrameric associative domains (AC_xA) examined by Shen et al. [34] The present materials approximately follow the expected scaling of the plateau modulus with the number of chains per unit volume: $PC_{30}P$ has almost twice the molecular weight of $PC_{10}P$, hence the 7% w/v gel of $PC_{30}P$ has approximately half the number concentration of chains and has approximately half the modulus of the 7% w/v $PC_{10}P$ gel. A stronger effect of midblock length is observed in the relaxation time of the gels, indicated by the frequency of the crossover of the elastic

modulus, G′, and the viscous modulus, G″; relaxation is fast enough to enable observation of terminal behavior at low frequencies for $PC_{10}P$, but not for $PC_{30}P$.

Collectively, the behavior of the plateau modulus and the relaxation time suggest complex changes in the network structure. The proportionality between linear elastic modulus and chain density implies that the topology of the network (e.g., fraction of elastically effective chains) is similar for $PC_{10}P$ and $PC_{30}P$ gels at 7% w/v, in contrast to the AC_xA materials in which increasing the midblock length strongly promotes the formation of elastically effective linkages.[34] Thus, the choice of endblock (P vs. A) qualitatively changes the effects of increasing midblock length on the plateau modulus. The profound effect of the endblock results from the discreteness of the aggregation number and the specificity of association (bias in favor of parallel vs. antiparallel) of the coiled-coil proteins. While the moduli suggest similarities in the network structure between $PC_{10}P$ and $PC_{30}P$, the increase in relaxation time from $PC_{10}P$ to $PC_{30}P$ suggests that the slowest relaxation process is qualitatively different in the two networks. This is in contrast to the expectation that the kinetics of a single coiled-coil exchange should be independent of the molecular weight of the midblock. Taken together, these results illustrate the interplay between endblock structure and midblock length that govern the network structure and properties of artificial protein hydrogels.

Strain sweeps at 1 rad/s (Figures 2c & d) show that the linear regime extends to approximately 50% strain amplitude in both materials. Further increase in strain amplitude produces a sharp decrease in the amplitude of the stress response, which also becomes nonsinusoidal. Nevertheless, the first harmonic dominates throughout the range of strain amplitude explored (γ_o<1000%). The abrupt decrease in the amplitude of the first harmonic, σ_1, occurs over a narrow range of γ_o (triangles, Figure 2, right), in which the character of the stress response changes from nearly elastic to predominantly dissipative: $G'_1(\gamma_o)$ decreases (circles) and G''_1 increases steeply (triangles) to meet G'_1. The increase in energy dissipation at this transition correlates with disruption of non-covalent associations within the network. With further increase in γ_o the stress amplitude σ_1 remains approximately constant. This stress plateau indicates an inverse relationship between strain amplitude and complex modulus, i.e., $|G^*_1|$ decreases as $1/\gamma_o$.[43] Since G''_1 dominates $|G^*_1|$, it scales approximately as $G''_1 \propto \gamma_o^{-1}$ (Figure 2, left), as observed previously by other authors.[43] (In the present materials, there is a slight increase of σ_1 with γ_o, approximately omega;$_1 \propto \gamma_o^{0.1}$, so $G''_1 \propto \gamma_o^{-0.9}$.) In the high-$\gamma_o$ plateau, G'_1 also falls as a power of γ_o—with an exponent that is twice that for G''_1 (note slopes of −1.8 in G′ and −0.9 in G″ in both Figures 2c&d). The stress curves $\sigma_1(\gamma_o)$ of both materials are consistent with a yielding response with a characteristic yield stress ≈ 1400 Pa and plateau stress ≈ 550 Pa at high γ_o. Notably, although the equilibrium modulus of the $PC_{10}P$ gel is greater than that of $PC_{30}P$, the yield stresses and plateau stresses of the two materials are approximately the same; the origin of the common yield stress is not clear.

Characteristics of yielding behavior are also evident in the shape of the non-sinusoidal stress response at high strain: Lissajous figures recorded in large amplitude oscillatory shear (LAOS) flow clearly become flattened (Figure 3) at high strain amplitudes, with the stress roughly constant with increasing strain during the oscillation, consistent with a yielding response.[44, 45] For comparison, at low strains the Lissajous figure is simply a line having a slope that reflects the linear viscoelastic properties of the gel at the test frequency.

The speed with which these telechelic protein hydrogels recover their full elastic strength is exceptional (Figure 4). After LAOS at strain amplitudes up to 500% (1 rad/s), $PC_{10}P$ recovers to approximately 98% of its initial elastic modulus nearly instantaneously. While $PC_{30}P$ shows a small permanent drop in the elastic modulus after the first LAOS strain

cycle, the modulus does not decrease further after subsequent strain cycles of increasing amplitude. Although the yielding mechanism that results in shear thinning in these protein hydrogels may play a role in self healing, comparison to other telechelic protein hydrogels and block copolymer hydrogels suggests that this rapid recovery is a property of the coiled-coil endblocks, since alternative endblocks lead to slower healing kinetics.[46] The time-dependent rheological response for $PC_{10}P$ illustrates that, in addition to rapid recovery, the onset of shear thinning is rapid (Figure 5). The gels show a noticeable time decay of the modulus only for relatively low strain amplitudes near the end of the linear regime. The combination of extreme shear thinning with rapid recovery of mechanical strength allows these gels to be injected through narrow (22 gauge) needles with only gentle hand pressure and formed into self-supporting structures, such as the free-standing arch shown in Figure 4.

In order to investigate the nature of the yielding behavior, the velocity profile during capillary flow of a $PC_{10}P$ hydrogel was visualized in a confocal microscope using fluorescent microspheres as flow markers.[42] A series of line scans was acquired at a rate of 500 scans/s at a fixed axial position approximately 50 diameters from the capillary entrance. Particle velocities are visualized by composing the scan lines as time-sequential columns of pixels in an image (Figure 6, top), with position along the diameter of the capillary along the vertical axis and time along the horizontal axis. Particles that move more slowly intercept the line scan for a longer time and appear more elongated in the time dimension than fast particles, which appear compressed in the time direction. Each discernable particle in the image was measured and its size in pixels was converted to a velocity using the known diameter of the particles. Particles move with an average velocity of 0.151 mm/s, corresponding to a flow rate of 4.5 μL/min, and the standard deviation of the velocity distribution is 15% of the mean. The average particle velocity does not vary with distance from the center of the capillary, indicating a plug flow velocity distribution. This suggests that gel in a solid-like state is flowing through the central region of the capillary due to yielding at or near the wall, which may be consistent with either wall slip or localized yielding near the wall within a narrow region of gel.

To distinguish whether shear banding or wall slip is the dominant mechanism for yielding, the gap thickness of the sample was varied in a parallel-plate geometry. These experiments show that the stress-strain curves are essentially independent of gap thickness, indicating that the yielding behavior is predominantly due yielding within the bulk of the material (supplemental information). Increased energy dissipation at the yield point also indicates yielding within the bulk of the gel, and a qualitatively similar rheological response has been observed in colloidal silica gels.[47] In the colloidal gels slip was minimized by the use of serrated plates, and the yielding behavior accompanied by the increase in G″ was attributed to network rupture. It is hypothesized that similar network rupture effects occur in the protein system due to dissociation of the coiled-coil protein endblocks under the high shear rates in a shear band. Given the density of chains in the system and the fact that the coiled-coil endblocks have interaction energies several times greater than the thermal energy, kT, the peak in G″ is small compared to the energy per unit volume of the coiled-coil linkages; therefore, dissociation of the coiled-coils within a small volume is consistent with the observed magnitude of the peak in G″. The largest loss modulus is observed at the lowest strain amplitudes, consistent with the inability of chains to rapidly reassociate in high shear flows.

Yielding within the gel indicates the onset of shear banding,[21, 48, 49] a phenomenon commonly observed in entangled polymer melts,[50, 51] DNA solutions,[23] wormlike micellar solutions,[22, 52–54] telechelic polymers,[46, 55] and micellar solutions crosslinked by telechelic polymers[56, 57] in both steady shear and LAOS. In the solid-like gel above the yield stress, strain is localized in regions where the crosslinks or entanglements are depleted, allowing

the intervening regions to move in a solid-like manner that maintains their crosslinked structure. The plateau in first harmonic stress results from yielding within this less entangled region. The overshoot in stress also suggests an activation barrier to shear thinning that is consistent with the nucleation hypothesis of shear band formation.[58] Because shear banding often results from a nonmonotonic stress-strain relationship, the stress in a homogeneous material may be increased into a metastable region, resulting in a stress drop after nucleation of a shear band.

Recently, the relationship between fracture and shear banding in transient networks has also been explored, and it has been shown that the microscopic fracture mechanism can be modeled with Griffith crack theory.[57] Crack growth in previously investigated hydrogels is visually observable, confirming the fracture mechanism. In these micellar solutions crosslinked by telechelic polymers, a plateau region has been observed even during unsteady shear banding.[56] Fracture was also observed in a telechelic protein using collagen helices as the associating groups investigated by Skrzeszewska et al.,[46] but in contrast to the transient micellar networks a plateau in stress was not observed with increasing strain rate with the collagen telechelic proteins. In the case of our coiled-coil protein hydrogels, visual observation during shear (using a transparent lower plate) shows no indication of fracture or void formation, and a plateau is observed after yielding. Sprakel et al.[59] show with particle-based simulations that a transition between shear banding and fracture may occur with increasing concentration; therefore, the absence of fracture in the coiled-coil protein gels considered here may indicate that the concentration of protein is below the transition from shear banding to fracture.

As noted earlier, shear banding is of interest in injectable gels for tissue engineering matrices, because it may allow seeded cells to survive the injection process. To evaluate the ability of the present coiled-coil protein gel to protect cells during injection, CHO K1 cells were seeded into a $PC_{30}P$ gel by allowing lyophilized protein to hydrate around the cells, and the cells were stained for viability after injection of the gel at a rate of approximately 5 mL/min (corresponding to a mean velocity of 0.43 m/s and nominal shear rate of 875 1/s). Cell survival was greater than 95% after injection and was not significantly different from that observed in the uninjected control (Figure 7). Negative controls with fixed cells show that the staining conditions are sufficient to identify dead cells. EthD dye non-specifically adhered to the protein gel, showing that the cells were encapsulated within the gel. Although relatively high shear stresses are required to induce shear thinning these gels, the shear-banding flow mechanism localizes the deformation to small regions of the gel. This allows a majority of seeded cells to experience extremely low shear strain and ensures high cell survival rates, in addition to allowing flow during injection.

Conclusions

A system of telechelic proteins with associating coiled-coil endblocks and a flexible polyelectrolyte midblock was used to formulate shear thinning injectable hydrogels. The materials demonstrate up to three orders of magnitude drop in their elastic modulus with increasing shear due to a sharp transition from a linear elastic solid to yielding flow. Genetic engineering of the protein can be used to control the physical properties of the gel such as changing modulus with changing midblock length without affecting the yielding behavior responsible for shear thinning. Flow visualization and LAOS rheology were used to characterize the yielding behavior, demonstrating that it is consistent with the formation of shear bands within the hydrogel. The extreme shear thinning and nearly instantaneous recovery to full elastic strength after the cessation of shear make these materials easy to inject and to sculpt into self-supporting structures for application as tissue engineering

matrices. The shear banding flow mechanism localizes strain into small volumes of the gel, allowing very high survival of encapsulated cells.

Supplementary Material

Refer to Web version on PubMed Central for supplementary material.

Acknowledgments

This work was supported by the NSF Center for the Science and Engineering of Materials and NIH Grant EB1971. BDO was supported by award number F32GM0834 from the National Institute of General Medical Sciences and by a Beckman Institute Postdoctoral Fellowship. We thank Professor S.E. Fraser for suggesting the method of flow visualization reported in Figure 3.

References

1. Yu L, Ding JD. Chem Soc Rev 2008;37(8):1473–1481. [PubMed: 18648673]
2. Mano JF. Adv Eng Mater 2008;10(6):515–527.
3. Peppas NA, Huang Y, Torres-Lugo M, Ward JH, Zhang J. Annu Rev Biomed Eng 2000;2:9–29. [PubMed: 11701505]
4. Sakiyama-Elbert SE, Hubbell JA. Annu Rev Mater Res 2001;31:183–201.
5. Engler AJ, Sen S, Sweeney HL, Discher DE. Cell 2006;126(4):677–689. [PubMed: 16923388]
6. Burdick JA, Anseth KS. Biomaterials 2002;23(22):4315–4323. [PubMed: 12219821]
7. Holland TA, Tabata Y, Mikos AG. J Control Release 2003;91(3):299–313. [PubMed: 12932709]
8. Shu XZ, Liu YC, Palumbo FS, Lu Y, Prestwich GD. Biomaterials 2004;25(7–8):1339–1348. [PubMed: 14643608]
9. Stile RA, Burghardt WR, Healy KE. Macromolecules 1999;32(22):7370–7379.
10. Bhattarai N, Ramay HR, Gunn J, Matsen FA, Zhang MQ. J Control Release 2005;103(3):609–624. [PubMed: 15820408]
11. Jeong B, Bae YH, Lee DS, Kim SW. Nature 1997;388(6645):860–862. [PubMed: 9278046]
12. Chiu YL, Chen SC, Su CJ, Hsiao CW, Chen YM, Chen HL, Sung HW. Biomaterials 2009;30(28): 4877–4888. [PubMed: 19527916]
13. Ramachandran S, Tseng Y, Yu YB. Biomacromolecules 2005;6(3):1316–1321. [PubMed: 15877347]
14. Gupta D, Tator CH, Shoichet MS. Biomaterials 2006;27(11):2370–2379. [PubMed: 16325904]
15. Haines-Butterick L, Rajagopal K, Branco M, Salick D, Rughani R, Pilarz M, Lamm MS, Pochan DJ, Schneider JP. P Natl Acad Sci USA 2007;104(19):7791–7796.
16. Liu XL, Mao YG, Mathias EV, Ma C, Franco O, Ba Y, Kornfield JA, Wang TL, Xue LJ, Zhou BS, Yen Y. J Sol-Gel Sci Techn 2008;45(3):269–278.
17. Ni XP, Cheng A, Li J. J Biomed Mater Res A 2009;88A(4):1031–1036. [PubMed: 18404710]
18. Li J, Ni XP, Leong KW. J Biomed Mater Res A 2003;65A(2):196–202. [PubMed: 12734812]
19. Liu KL, Zhu JL, Li J. Soft Matter 2010;6(10):2300–2311.
20. Moller PCF, Rodts S, Michels MAJ, Bonn D. Phys Rev E 2008;77(4):041507.
21. Olmsted PD. Rheol Acta 2008;47(3):283–300.
22. Walker LM. Curr Opin Colloid In 2001;6(5–6):451–456.
23. Boukany PE, Hu YT, Wang SQ. Macromolecules 2008;41(7):2644–2650.
24. Zhou, L.; Ewoldt, RH.; Cook, LP.; McKinley, GH. Probing shear-banding transitions of entangled liquids using Large Amplitude Oscillatory Shearing (LAOS) deformations. In: Co, A.; Leal, LG.; Colby, RH.; Giacomin, AJ., editors. XVth Int Congr Rheol - the Society of Rheology 80th Annual Meeting, Pts 1 and 2. Vol. 1027. 2008. p. 189-191.
25. Ravindranath S, Wang SQ. J Rheol 2008;52(2):341–358.
26. Petka WA, Harden JL, McGrath KP, Wirtz D, Tirrell DA. Science 1998;281(5375):389–392. [PubMed: 9665877]

27. Krishna OD, Kiick KL. Biopolymers Peptide Sci 2010;94(1):32–48.
28. Xu CY, Breedveld V, Kopecek J. Biomacromolecules 2005;6(3):1739–1749. [PubMed: 15877401]
29. Xu CY, Kopecek J. Pharm Res 2008;25(3):674–682. [PubMed: 17713844]
30. Shen W, Zhang KC, Kornfield JA, Tirrell DA. Nat Mater 2006;5(2):153–158. [PubMed: 16444261]
31. Yang JY, Xu CY, Wang C, Kopecek J. Biomacromolecules 2006;7(4):1187–1195. [PubMed: 16602737]
32. Yang JY, Xu CY, Kopeckova P, Kopecek J. Macromol Biosci 2006;6(3):201–209. [PubMed: 16514591]
33. Wang C, Kopecek J, Stewart RJ. Biomacromolecules 2001;2(3):912–920. [PubMed: 11710049]
34. Shen W, Kornfield JA, Tirrell DA. Soft Matter 2007;3(1):99–107.
35. Shen, W. PhD Thesis. California Institute of Technology; Pasadena: 2005. Structure, Dynamics, and Properties of Artificial Protein Hydrogels Assembled Through Coiled-Coil Domains.
36. Nowak AP, Breedveld V, Pakstis L, Ozbas B, Pine DJ, Pochan D, Deming T. J Nature 2002;417(6887):424–428.
37. Wright ER, McMillan RA, Cooper A, Apkarian RP, Conticello VP. Adv Funct Mater 2002;12(2): 149–154.
38. Nagapudi K, Brinkman WT, Thomas BS, Park JO, Srinivasarao M, Wright E, Conticello VP, Chaikof EL. Biomaterials 2005;26(23):4695–4706. [PubMed: 15763249]
39. Nagapudi K, Brinkman WT, Leisen J, Thomas BS, Wright ER, Haller C, Wu XY, Apkarian RP, Conticello VP, Chaikof EL. Macromolecules 2005;38(2):345–354.
40. Martens AA, Portale G, Werten MWT, de Vries RJ, Eggink G, Stuart MAC, de Wolf FA. Macromolecules 2009;42(4):1002–1009.
41. Werten MWT, Teles H, Moers A, Wolbert EJH, Sprakel J, Eggink G, de Wolf FA. Biomacromolecules 2009;10(5):1106–1113. [PubMed: 19374376]
42. Jones EAV, Baron MH, Fraser SE, Dickinson ME. Am J Physiol-Heart C 2004;287(4):H1561–H1569.
43. Li X, Wang SQ, Wang XR. J Rheol 2009;53(5):1255–1274.
44. Ewoldt, RH.; Hosoi, AE.; McKinley, GH. An ontology for large amplitude oscillatory shear flow. In: Co, A.; Leal, LG.; Colby, RH.; Giacomin, AJ., editors. XVth Int Congr Rheol - the Society of Rheology 80th Annual Meeting, Pts 1 and 2. Vol. 1027. 2008. p. 1135-1137.
45. Ewoldt RH, Hosoi AE, McKinley GH. J Rheol 2008;52(6):1427–1458.
46. Skrzeszewska PJ, Sprakel J, de Wolf FA, Fokkink R, Stuart MAC, van der Gucht J. Macromolecules 2010;43(7):3542–3548.
47. Walls HJ, Caines SB, Sanchez AM, Khan SA. J Rheol 2003;47(4):847–868.
48. Milner ST, McLeish TCB, Likhtman AE. J Rheol 2001;45(2):539–563.
49. Adams JM, Olmsted PD. Phys Rev Lett 2009;102(6):067801. [PubMed: 19257634]
50. Tapadia P, Ravindranath S, Wang SQ. Phys Rev Lett 2006;96(19):196001. [PubMed: 16803112]
51. Olmsted PD, Radulescu O, Lu CYD. J Rheol 2000;44(2):257–275.
52. Salmon JB, Colin A, Manneville S, Molino F. Phys Rev Lett 2003;90(22):228303. [PubMed: 12857346]
53. Berret JF, Roux DC, Porte G. J Phys II 1994;4(8):1261–1279.
54. Spenley NA, Cates ME, McLeish TCB. Phys Rev Lett 1993;71(6):939–942. [PubMed: 10055406]
55. Sprakel J, Spruijt E, Stuart MAC, Besseling NAM, Lettinga MP, van der Gucht J. Soft Matter 2008;4(8):1696–1705.
56. Michel E, Appell J, Molino F, Kieffer J, Porte G. J Rheol 2001;45(6):1465–1477.
57. Tabuteau H, Mora S, Porte G, Abkarian M, Ligoure C. Phys Rev Lett 2009;102(15):155501. [PubMed: 19518646]
58. Dhont JKG, Briels WJ. Rheol Acta 2008;47(3):257–281.
59. Sprakel J, Spruijt E, van der Gucht J, Padding JT, Briels WJ. Soft Matter 2009;5(23):4748–4756.

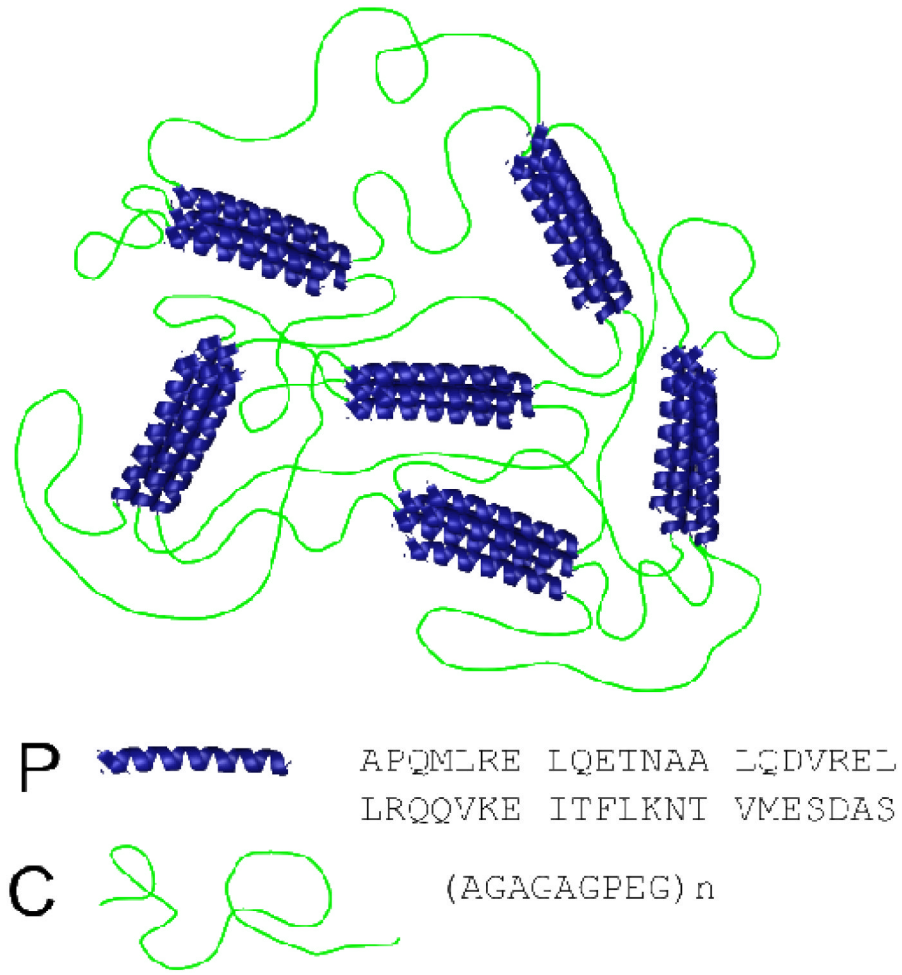

Figure 1. Structure of telechelic protein hydrogels

Telechelic proteins with coiled-coil endblocks and flexible polyelectrolyte midblocks associate in solution to form networks with junctions defined by the coiled-coil association state and connected by monodisperse linkers.

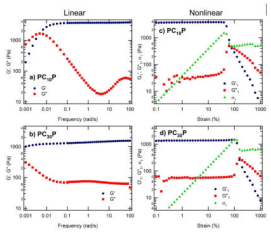

Figure 2. Linear and nonlinear rheology of PCP hydrogels

The linear dynamic moduli (left), elastic modulus, G′(ω) and loss modulus, G″ (ω), and the nonlinear strain-dependence of the first harmonic component of the stress (right), $\sigma_1 \equiv |\sigma^*_1(\gamma_o)|$, $G'_1(\gamma_o)$ and $G''_1(\gamma_o)$ at a fixed ω=1 rad/s, for $PC_{10}P$ (top) and $PC_{30}P$ (bottom) hydrogels that were prepared in 100 mM phosphate buffer, pH 7.6, at 7% w/v concentration. In the linear regime (left), each gel exhibits a plateau modulus at high frequency and a characteristic relaxation time that depends on the midblock length. At a fixed frequency of 1 rad/s, increasing the strain amplitude reveals a yield stress above which the gels shear thin by three orders of magnitude.

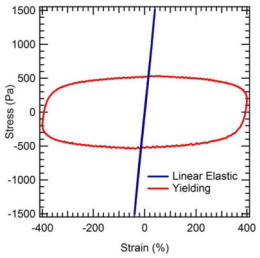

Figure 3. Lissajous figures for $PC_{10}P$

At low strain amplitude the material shows linear curves characteristic of an elastic solid, while at high strain a flattened ellipse is observed, indicative of yielding behavior. Curves are acquired at 1 rad/s for a 7% gel in 100 mM phosphate buffer at pH 7.6.

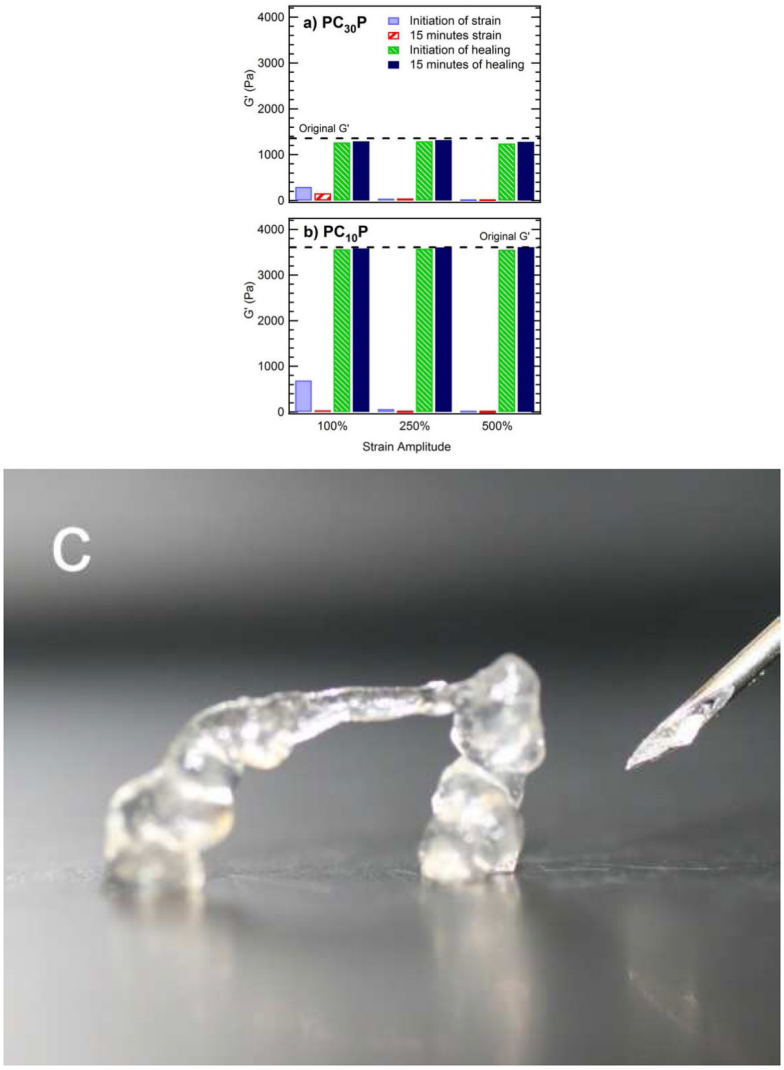

Figure 4. Rapid recovery of hydrogels after large amplitude oscillatory strain (LAOS)

(a) $PC_{30}P$ recovers over 90% of its undisrupted modulus within seconds (the time required to record the first measurement at small strain, 0.1%) after the cessation of LAOS, independent of the imposed strain amplitude. (b) $PC_{10}P$ recovers over 98% of its original modulus within the first measurement time, with greater than 99% recovery after 15 minutes. The measurement frequency was 1 rad/s for both samples. (c) The fast recovery of $PC_{10}P$ allows self-supporting structures to be produced.

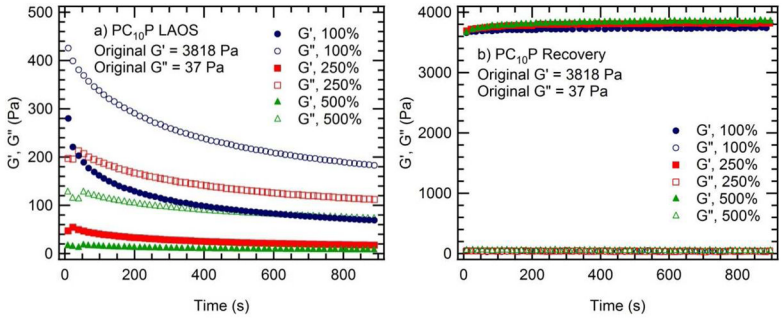

Figure 5. Time decay and recovery of mechanical properties for $PC_{10}P$ under large amplitude oscillatory shear

Measurements were performed at 1 rad/s. LAOS was performed for 15 minutes at the indicated strain amplitude, and recovery was conducted for 15 minutes at 0.1% strain amplitude.

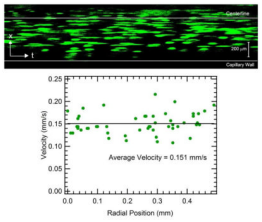

Figure 6. Visualization of the flow profile in capillary flow of a $PC_{10}P$ hydrogel labeled with fluorescent microsphere tracers

Time-dependent line scans along the diameter of a capillary (1.93 ms/scan) show that the transit time for a particle to cross the plane of the line scan is approximately the same for all distances from the center of the capillary, indicating a plug flow type profile. This implies yielding in the gel layer adjacent to the capillary wall, consistent with the shear banding mechanism.

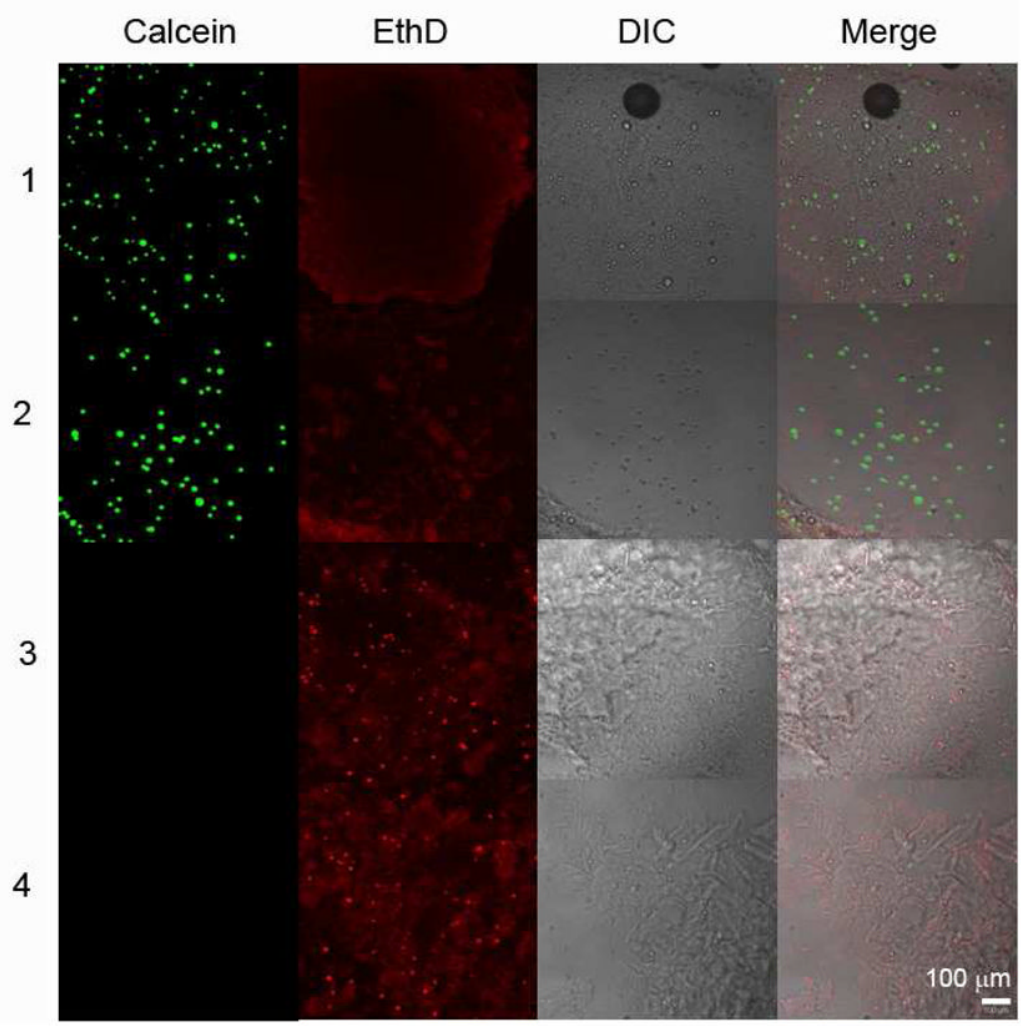

Figure 7. Cell survival after injection in a $PC_{30}P$ hydrogel matrix

The live/dead cell assay indicates greater than 95% cell survival after the acute shear stress of injection. (1) Live cells without injection; (2) Live cells after injection; (3) Fixed cells without injection; (4) Fixed cells after injection. Calcein stain identifies live cells, while EthD stain identifies dead cells and adheres non-specifically to the hydrogel.